ACS SENSORS

pubs.acs.org/acssensors

Article

High-Performance Field-Effect Sensing of Ammonia Based on High-Density and Ultrathin Silicon Nanowire Channels

Chunsheng Yang, Wei Liao, Junzhuan Wang, and Linwei Yu*

Cite This: *ACS Sens.* 2024, 9, 6284−6291

Read Online

ACCESS | Metrics & More | Article Recommendations | Supporting Information

ABSTRACT: Ultrathin silicon nanowires (SiNWs), grown via a high-yield and low-cost catalytic approach, are ideal building blocks for the construction of highly sensitive field-effect transistor (FET) sensors. In this work, we demonstrate a high-density growth integration of an ultrathin SiNW array, with diameter down to D_{NW} = 24 ± 3 nm and narrow NW-to-NW spacing of only 120 nm, fabricated via an in-plane solid−liquid−solid (IPSLS) approach. Junctionless bottom-gated SiNW FETs are successfully constructed, exhibiting a high on/off current ratio of >10^7 and a sharp subthreshold swing of 156 mV/dec These provide an excellent platform for realizing high-performance NH_3 sensing at room temperature, with a high response of 96.9% at 25 ppm and 38.6% at 2.5 ppm, rapid response time of 7.9 s for 5% response (or 85.8 s for 50% response), and superior selectivity against common volatile organic compound gases in ambient environments. Finally, the field-effect sensing mechanism is attributed to the Schottky barrier modulation by the adsorbed NH_3 molecules at the metal/SiNW interface, as confirmed through an epoxy-masked selective region comparative analysis. These results provide a solid basis for the ultrathin catalytic IPSLS-SiNWs to serve as advantageous one-dimensional (1D) channels for the scalable integration of various high-performance and flexible gas sensing applications.

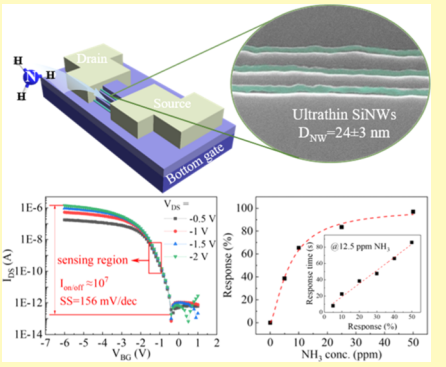

KEYWORDS: *ultrathin SiNW FET, NH_3 gas sensor, in-plane solid−liquid−solid, Schottky barrier modulation*

In recent decades, the burgeoning demand for toxic and hazardous gas detection in pollution monitoring, industrial processes, agricultural production, medical diagnosis, and home safety[1−3] has catalyzed the swift advancement of various gas sensing technologies based on electrical,[4] electrochemical,[5] optical,[6] and acoustic[7] mechanisms. Among them, gas sensors based on changes in electrical properties have attracted widespread attention due to their advantages of simple detection, fast response, and low cost.[3] Especially, compared to traditional two-terminal devices,[8,9] field-effect sensors have enhanced gas sensing capabilities with advantages such as high sensitivity, rapid response, low power consumption, scalable integration, and strong anti-interference ability.[10,11] Therefore, many nanostructure materials, such as silicon nanowire (SiNWs),[12] carbon nanotubes,[13] metal-oxide semiconductors,[14] graphene,[15] and transition metal dichalcogenides,[16] have been widely researched as promising channels of field-effect transistor (FET) gas sensor. Particularly, SiNWs, with their relatively high carrier mobility, large specific surface area, and compatibility to mature Si technology, are ideal for creating label-free, real-time, and highly sensitive gas sensors.[17,18]

The diameter of SiNWs (D_{NW}) significantly influences the performance of gas sensors, as a reduction in diameter enhances response sensitivity due to an increased surface-to-volume ratio[19] and comparability to the Debye screening length.[20,21] Therefore, fabricating an ultrathin and uniform SiNW array is a key factor in optimizing the performance of gas sensors. The ultrathin SiNWs with diameters narrower than 30 nm can be produced via a top-down etching process, with the aid of high-resolution lithography, such as e-beam lithography (EBL) and deep ultraviolet (DUV) lithography, which are however costly and inefficient for large-area or flexible electronics. In contrast, another common technique is the bottom-up approach, famously the vapor−liquid−solid (VLS) growth method, but it is difficult to precisely position the VLS-grown SiNWs on a flat surface as they are usually produced as standing bundles. In order to address this challenge, an in-plane solid−liquid−solid (IPSLS) technology has been established in our previous works,[22−24] where indium catalyst droplets absorb amorphous silicon thin-film precursors to produce crystalline SiNW array. These orderly SiNWs have provided ideal one-dimensional (1D) channels for building high-performance FET gas sensors in the past decade.[8,25,26] However, the specific sensing activity region and the underlying sensing mechanism for the label-free Schottky-

Received: September 9, 2024
Revised: October 19, 2024
Accepted: November 1, 2024
Published: November 8, 2024

https://doi.org/10.1021/acssensors.4c02426
ACS Sens. 2024, 9, 6284−6291

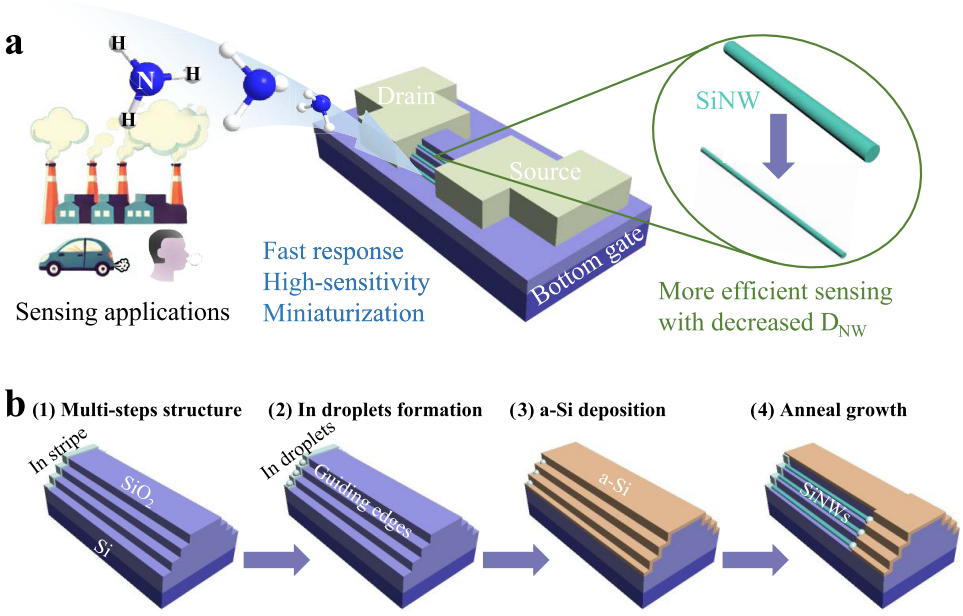

Figure 1. (a) Schematic illustration of highly sensitive SiNW FET ammonia sensing constructed upon high-density and ultrathin SiNWs under the control of the bottom gate. (b) Fabrication procedure of the guided growth of the orderly SiNW array via an IPSLS mechanism.

contacted SiNW FET gas sensors at room temperature have remained unexplored until now.

In this work, we utilized an IPSLS technique[22] for the growth of SiNWs, applied a multisteps structure technique[27] to narrow the NW-to-NW spacing to only 120 nm, and minimize the D_{NW} to 24 ± 3 nm by refining the size of the indium catalyst and the thickness of the amorphous silicon layer. Based on bottom-gated SiNW FET, exhibiting a high on/off current ratio of $>10^7$ and a sharp subthreshold swing of 156 mV/dec, as depicted in Figure 1a, high-performance NH_3 sensing has been accomplished at room temperature, with a high response of 96.9% at 50 ppm (ppm) and 38.6% at 2.5 ppm, rapid response time of 7.9 s for 5% response (or 85.8 s for 50% response), and superior selectivity against common volatile organic compound (VOC) gases in ambient environments. More importantly, we have designed and conducted an epoxy-masked selective region comparative experiment to clarify the field-effect sensing mechanism of these Schottky-contacted SiNW FET sensors, which is fundamentally important for improving future sensing performance.

EXPERIMENTAL SECTION

Growth of SiNWs by IPSLS. The SiNWs grew on a multisteps structure (explored in previous work[27]) with three-layered guiding edges through an IPSLS growth mechanism, as shown in Figure 1b. A strip of metal indium, 5 nm in thickness, was evaporated at the end of the multisteps guiding channels using conventional lithography, followed by thermal evaporation (TE) and a lift-off process. Subsequently, the oxidized indium strip was treated in a plasma-enhanced chemical vapor deposition (PECVD) system at 250 °C for 4 min using a hydrogen plasma with a flow rate of 14.8 sccm, chamber pressure of 140 Pa, and a radio frequency (RF) power of 10 W. This treatment reduced and condensed the oxidized indium strip into catalytic indium droplets. At 100 °C and 20 Pa, an amorphous silicon film was deposited uniformly on the sample surface using 5 sccm SiH_4 for 2 min with an RF power of 2 W. The substrate was then heated to 350 °C to activate the molten indium droplets, and this condition was maintained under vacuum for 1 h. During the IPSLS growth, due to the difference in Gibbs free energy between crystalline silicon and amorphous silicon, the catalytic indium droplets rolled along the guiding edges and catalyzed the transformation of amorphous silicon into crystalline silicon. In this way, high-density and ultrathin SiNWs were obtained. It is noteworthy that D_{NW} can be precisely controlled by the thickness of the amorphous silicon film and the size of the indium strip.[28,29] The sample surface was treated with CF_4 plasma in a reactive ion etching (RIE) machine for 3 min at 4 Pa, with a flow rate of 30 sccm and a power of 5 W, to remove the residual amorphous silicon. Then, the sample was annealed in an oxidation furnace under dry oxygen conditions at 850 °C for 5 min to further reduce D_{NW} and minimize the density of SiNW defects.

Fabrication of SiNW FET Sensor. After defining the source and drain electrode patterns through photolithography, the sample was soaked in a buffer oxide etch (BOE) solution for approximately 4 s to remove the native oxide layer on the surface of the SiNWs. Following this, in an electron beam evaporation (EBE) system, metal platinum and aluminum with thicknesses of 5 and 55 nm, respectively, were sequentially evaporated onto the sample surface, and the source and drain electrodes of SiNW FET were fabricated through a lift-off process. The oxide layer on the silicon wafer surface was disrupted, and a conductive silver paste was used to connect the p^+-Si at the bottom of the substrate as a bottom gate. In this way, a high-density SiNW FET sensor array was obtained.

Real-Time Gas-Sensitive Detection. The performance of the SiNW FET sensor was assessed by using a dynamic intelligent gas sensing measurement system, as depicted in Figure S1. This system included a stainless test chamber with a capacity of approximately 2.4 L, a gas source, a mixing chamber, and a source meter (Keysight 2636B), all operated at room temperature (25 °C). The gas source supplied two types of gases: dry high-purity air with a N_2-to-O_2 ratio of 79:21, and NH_3 gas diluted in N_2 at a concentration of 0.5%. The mixing chamber employed mass-flow controllers (MFCs) to regulate the flow of these gases, ensuring a steady supply of NH_3 gas at a predetermined concentration in the test chamber. Throughout the testing process, the total gas flow was maintained at 2000 sccm. The flow rate of the diluted NH_3 gas was controlled between 1 and 10 sccm, corresponding to a concentration range of 2.5−25 ppm. To evaluate the NH_3 response of sensor under various gate biases, the bottom-gated SiNW FET was biased with a drain-source voltage (V_{DS}) of −0.5 V and bottom gate voltage (V_{BG}) of −1.0, −1.5, or −2.0 V, all at 25 °C. The response (R) of the sensor to NH_3 is defined as

https://doi.org/10.1021/acssensors.4c02426
ACS Sens. 2024, 9, 6284−6291

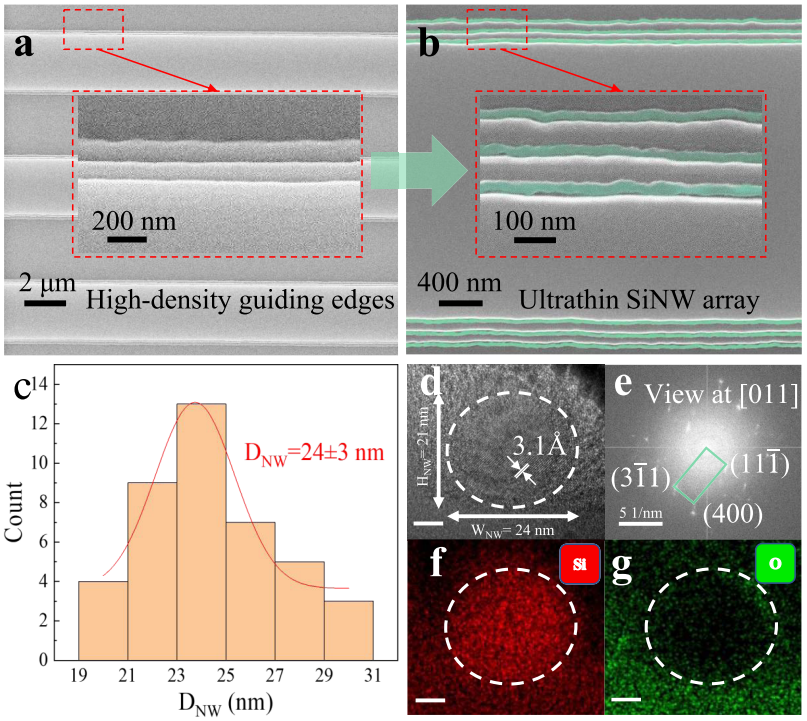

Figure 2. Typical top-view SEM images of (a) multistep structure with three-layered guiding edges and (b) high-density and ultrathin SiNW array with (c) diameter distribution of 24 ± 3 nm. (d) HR TEM characterizations of the cross section of the single SiNW and (e) FFT diffraction patterns of the lattice image. EDS analysis of the cross section of the single SiNW, with separate elemental distributions of the (f) Si and (g) O atoms. The scale bars in (d, f, g) both stand for 5 nm.

$$R = \left| \frac{I - I_0}{I_0} \right| \times 100\% \quad (1)$$

where I_0 and I represent the initial current of the sensor in dry air and the response current during exposure to diluted NH_3 gas, respectively. Additionally, the reversibility of the sensor was verified through cyclic testing with 12.5 ppm of ammonia and high-purity air. The sensor selectivity was evaluated by its response to 25 ppm of ammonia and VOC gases. The VOCs were introduced by injecting them into a vaporizer using a syringe pump and then carried into the chamber with high-purity air at the same concentration and flow rate.

RESULTS AND DISCUSSION

Characterization of SiNWs. Figure 2a presents the typical top-view scanning electron microscopy (SEM) image of the multistep structure with three-layered guiding edges. Each step has a height of approximately 80 nm and a width of 120 nm as measured by a step profiler. The width of steps indirectly determines the size of condensed catalyst indium droplet, which affects the diameter of the grown SiNWs. The SiNWs grew stably along the guiding edges of the multistep structure, where the ultrathin SiNWs were highlighted in green for ease of observation, as shown in Figure 2b. The D_{NW} is about 24 ± 3 nm, and the specific statistical data is shown in Figure 2c, which essentially conforms to a Gaussian distribution. To examine the crystalline structure of the SiNWs, their cross-sectional profiles were exposed by focused ion beam (FIB) milling and then analyzed by high-resolution transmission electron microscopy (HR TEM). As depicted in Figure 2d, the crystalline SiNWs were marked with white dashed lines, showing that the width and height of the SiNW are 24 and 21 nm, respectively, which is consistent with the SEM top-view result. The presence of amorphous silicon is also observed at the top and outer edges of the SiNWs, which is residual amorphous silicon from the growth process. A typical interplanar spacing of 3.1 Å indicates the presence of the Si (111) crystal plane. After further fast Fourier transform (FFT) processing, the result shown in Figure 2e confirms that the SiNWs grew in the Si <100> crystallographic orientation. The elemental distribution of the cross-sectional profiled in Figure 2f,g also confirms the existence of SiNWs via energy dispersive spectrometer (EDS) analysis.

Performance of SiNW FET Ammonia Sensor. Figure 3a presents an optical image of the fabricated bottom-gated SiNW FFT array with a channel length of approximately 15 μm. The transfer characteristic curve is depicted in Figure 3b, where the SiNW FET exhibits a high on/off ratio of $>10^7$, and a sharp subthreshold swing of 156 mV/dec, indicative of typical p-type channel behavior. This is attributed to the incorporation of indium atoms into the SiNWs during the growth process of IPSLS, serving as p-type dopants within the SiNWs. The output characteristic curve, as shown in Figure 3c, demonstrates a clear dependence of the current on the gate bias applied, confirming the pronounced field effect. Notably, the SiNW FET sensors showed a distinct response to target NH_3 molecules without any modification. The sensing performance was measured under a V_{DS} of −0.5 V, with a tunable V_{BG} of −1.5 V, targeting a working regime with an initial channel current of approximately 1.70 nA, as highlighted by the red rectangle in Figure 3b. In this work, all tests were conducted at 25 °C, using dry high-purity air as the background carrier gas at a total flow rate of 2000 sccm, which was maintained throughout the process.

Figure 3d presents the sensing properties of SiNW FET sensors upon exposure to NH_3 gas over a range of concentrations from 2.5 to 25 ppm. To better illustrate the changes in the response current, the y-axis was transformed

https://doi.org/10.1021/acssensors.4c02426
ACS Sens. 2024, 9, 6284−6291

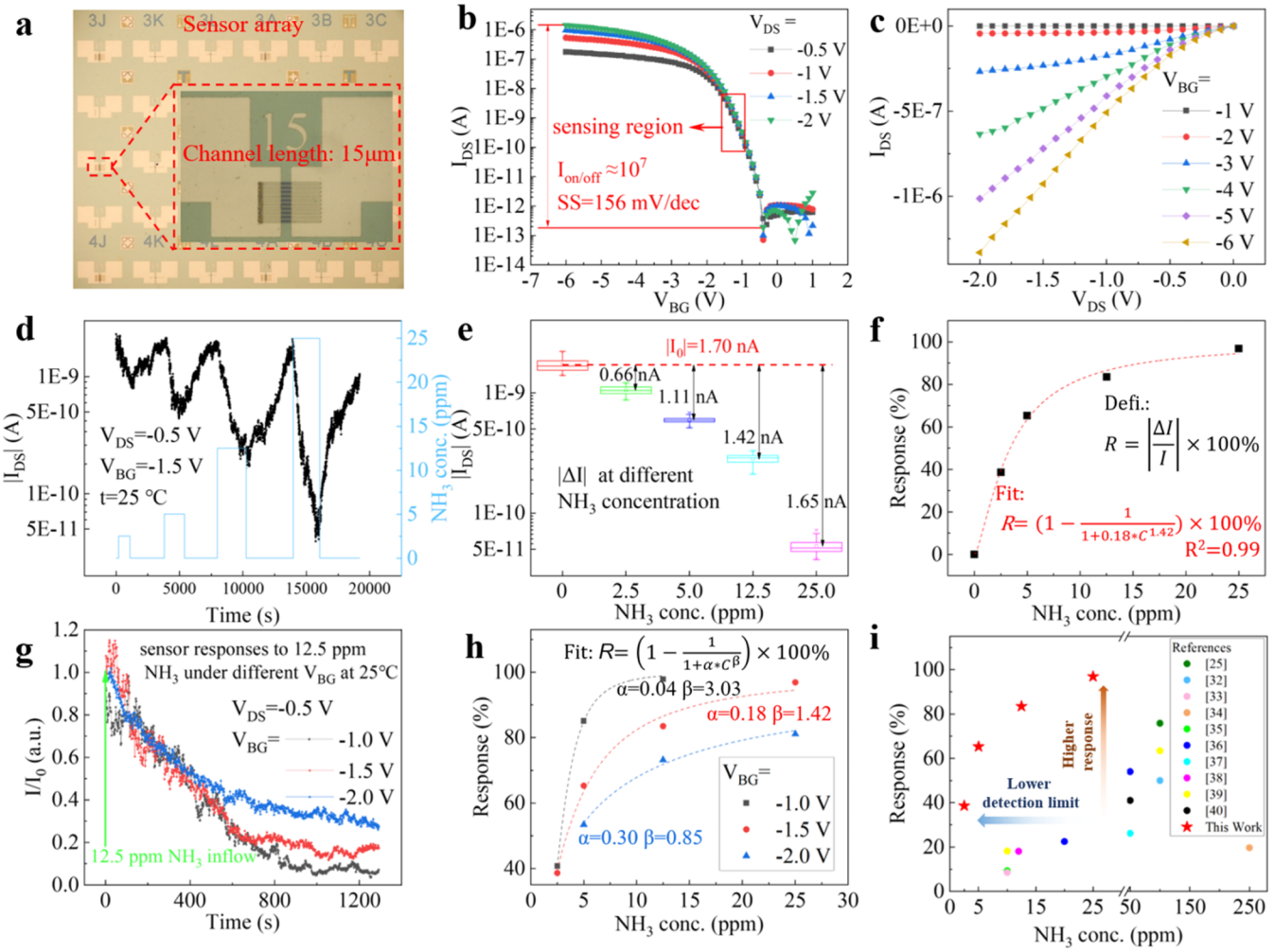

Figure 3. (a) Optical image of the SiNW FET sensor array, with the inset showing the channel length is 15 μm. Electrical transport and NH_3 gas sensing properties of the SiNW FET sensors: (b) the typical transfer curve and (c) the output curve of the bottom-gated SiNW FET. (d) Dynamic response of the sensor to NH_3 gas at 25 °C with V_{DS} = −0.5 V and V_{BG} = −1.5 V. (e) Absolute value of the response current change ($|\Delta I|$) for the sensor at different NH_3 concentrations via statistical calculation of (d). (f) Dependence of NH_3 concentration on the response and the corresponding nonlinear fitting. (g) Dynamic response of the sensor to 12.5 ppm of NH_3 and (h) nonlinear fitting in their respective ranges under various V_{BG}. (i) Response comparison of reported NH_3 gas sensors based on SiNWs or other semiconductor materials.

into a logarithmic scale. The SiNW FET sensor showed a strong decrease in conductance to NH_3 gas (p-type sensing behavior), indicating that the charge carrier transport channel was impeded by the adsorption of NH_3 molecules. Additionally, there was a corresponding decline in the responsive channel current with a rise in the NH_3 gas concentration from 2.5 to 25 ppm. Remarkably, the change in the response current reached about 2 orders of magnitude at 25 ppm of NH_3. Upon cessation of the NH_3 gas supply, the current was able to return to its initial value, indicating that the charge carrier transport channel recovered with the desorption of NH_3 molecules. The nanoscale metal/SiNW contact might also be susceptible to subtle environmental noises, leading to fluctuations during detection.[30] To mitigate the impact of environmental noise fluctuations on the test results, statistical processing of the data was performed. The absolute value of the initial current ($|I_0|$) was taken as the average of 100 current points measured with only high-purity air flowing, and the response current ($|I|$) was taken as the average of the last 100 current points before stopping the supply of the NH_3 gas. The change in response current (ΔI) at different NH_3 concentrations is defined as $\Delta I = I - I_0$. The statistical results are presented in Figure 3e, from which it can be deduced that the absolute values of the response current change ($|\Delta I|$) for the sensor at 2.5, 5, 12.5, and 25 ppm of NH_3 are 0.66, 1.11, 1.42, and 1.65 nA, respectively. The calculated results are depicted in Figure 3f, showing that the response of the sensor to 2.5 and 25 ppm of NH_3 is 38.6 and 96.9%, respectively. Usually, the response (R^*) of resistance-type semiconductor gas sensors is defined as the ratio of the resistance change in the target gas to the initial resistance in air, and it can be empirically represented by the formula[31]

$$R^* = \alpha P_g^{\beta} \tag{2}$$

where P_g is the target gas partial pressure, which is proportional to the gas concentration, α is a prefactor, and β is the exponent on P_g. Considering the case of a p-type FET gas sensor responding to reducing NH_3 gas, as the NH_3 concentration approaches infinity, the response tends to 100%. By analogy, the empirical formula is derived as

https://doi.org/10.1021/acssensors.4c02426
ACS Sens. 2024, 9, 6284−6291

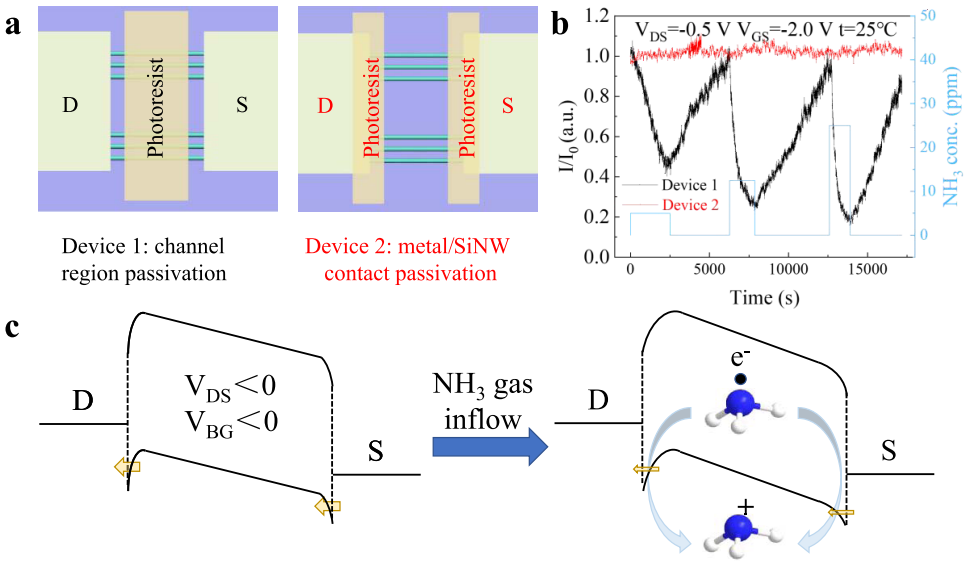

Figure 4. (a) Schematic illustration for Device 1 with photoresist-passivated SiNW channels and Device 2 with passivated metal/SiNW contact. (b) Sensing performance of Device 1 (responses normally as shown in the black lines) and Device 2 (almost no response as shown in the red line), respectively. (c) Energy band diagram of the sensor before and after exposure of NH_3 molecules.

$$R = \left(1 - \frac{1}{1 + \alpha P_g^{\beta}}\right) \times 100\% \tag{3}$$

Fitting the response of the sensor for different concentrations yields

$$R = \left(1 - \frac{1}{1 + 0.066 \times C^{1.42}}\right) \times 100\% \tag{4}$$

where C represents the NH_3 concentration, as shown in Figure 3f. The determination coefficient (R^2) is 0.99, indicating that the data points are tightly distributed in the vicinity of the fitting curve. Generally, the exponent β has an ideal value of 0.5 for resistance-type semiconductor gas sensors. In our case, the value of the sensitivity factor β is approximately 1.42 with a margin of error of ±0.12, which is significantly higher compared to that of resistance-type gas sensors. The improvement of sensitivity factor can likely be attributed to the field effect that even the slightest changes in surface charge can exert a pronounced impact on the internal current of SiNWs.

In fact, the sensing performance of the SiNW FET sensor can be modulated by the applied V_{BG} easily. Figure 3g typically illustrates the variation in the relative current response of the sensor to 12.5 ppm of NH_3 at various V_{BG}. It is observed that the sensor, operating closer to the subthreshold region, benefits from an enhanced subthreshold swing, thereby exhibiting a superior response to the same concentration of NH_3. However, the sensor is more susceptible to environmental noise fluctuations under lower V_{BG}, which may be one of the reasons the response speed does not show an advantage under this condition. The response of sensor to different NH_3 concentrations at various V_{BG} is summarized in Figure 3h (more details are shown in Figure S2). At a lower V_{BG}, represented by the black fitting curve, the sensor exhibits more sensitivity to NH_3 gas and achieves a response of 97.3% for 12.5 ppm of NH_3, albeit with a greater susceptibility to saturation. Conversely, at higher V_{BG}, indicated by the blue fitting curve, the sensor fails to detect a response even at 2.5 ppm of NH_3, and the response at various NH_3 concentrations is diminished. Nonetheless, a broader detection range can be obtained. Despite the limitation of the experimental platform to a maximum NH_3 concentration of 25 ppm at a total gas flow rate of 2000 sccm, this outcome is predictable easily. In summary, the limit of detection and detection range of the sensor can be modulated simply by adjusting the gate voltage, enabling the sensor to be situated in an appropriate sensing region.

Furthermore, compared with other reported NH_3 gas sensors based on SiNWs[25,32−34] or other semiconductor materials[35−40] (as shown in Figure 3i and Table S1), this SiNWs FET ammonia sensor exhibits a higher response and a lower detection limit. Particularly, for SiNWs-based NH_3 gas sensor, the improvement is attributed to the ultrathin SiNWs, which not only provides a larger surface-to-volume ratio but is also more comparable to the Debye screening length. This allows surface states caused by chemisorption to significantly change the electronic properties of the system, thereby leading to improved response.[20]

Sensing Mechanism for Schottky-Contacted SiNW FET Ammonia Sensor. To further investigate the underlying sensing mechanism of the sensor, two distinct devices including Devices 1 and 2 were designed, as depicted in Figure 4a. For Device 1, the central channel region was completely coated with photoresist, thereby exposing the Schottky junction for direct interaction with the NH_3 molecules. In contrast, Device 2 was engineered such that the Schottky junction was covered by the photoresist, leaving the channel region accessible for NH_3 gas exposure. This comparative design approach facilitated a systematic exploration of the contributions of the Schottky junction and the channel region to the response of the sensor. Subsequently, the NH_3 sensing responses of both devices were evaluated. Device 1, which had the Schottky junction exposed, demonstrated a typical current decrease upon NH_3 gas inflow and an increase upon outflow, as depicted by the black line in Figure 4b. Conversely, Device 2, with the channel region exposed, exhibited negligible variations in current in response to the

https://doi.org/10.1021/acssensors.4c02426
ACS Sens. 2024, 9, 6284−6291

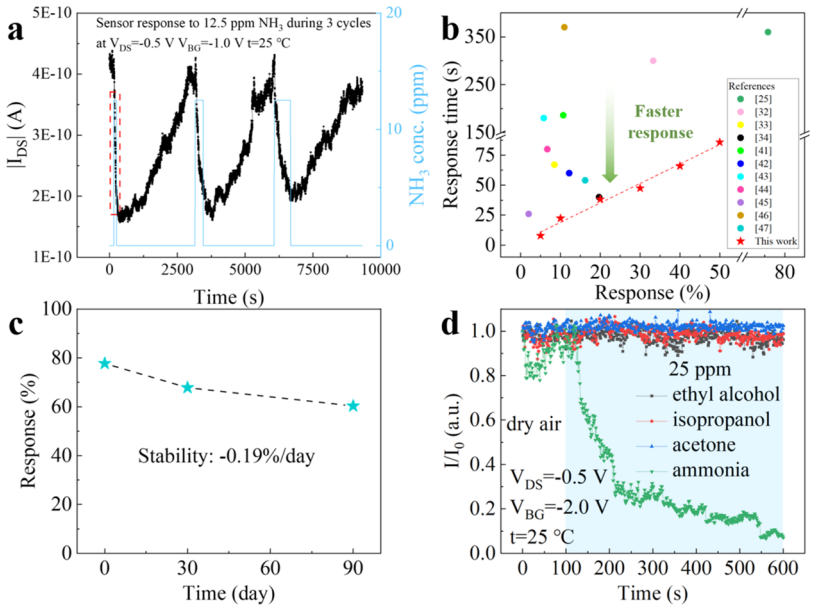

Figure 5. (a) Three cycles test result of the sensor to 12.5 ppm of NH_3. (b) Response time of the sensor for corresponding response during the first cycle of 5a and response time comparison of reported NH_3 gas sensors based on SiNWs or other semiconductor materials. (c) Stability of the SiNW FET ammonia sensor during three months. (d) Selectivity of the SiNW FET ammonia sensor against common VOC gases.

inflow and outflow of NH_3 gas, as represented by the red line in Figure 4b. These observations indicated that the Schottky junction played a predominant role in the sensing mechanism of the Schottky-contacted SiNW FET sensor at room temperature, with the channel region contributing minimally to the observed sensing behavior. Herein, a reasonable field-effect sensing mechanism for NH_3 detection using the Schottky-contacted SiNW FET sensor is proposed, as depicted in Figure 4c. At room temperature, an appropriate V_{DS} and a negative V_{BG} are applied to the p-type SiNW FET. This application elevates the energy band of the SiNW, resulting in an increased height of the Schottky barrier, but more significantly, it reduces its thickness. Consequently, the carrier is enabled to tunnel through the Schottky barrier, switching the device to an on-state. In Device 1, when reductive NH_3 molecules are adsorbed onto the Schottky junction area, they readily lose an electron to become positively charged NH_3 ions. This process increases the thickness of the Schottky barrier, significantly reducing the probability of charge carrier tunneling through it, which results in a substantial decrease in the channel current. In Device 2, the photoresist impedes the influence of NH_3 molecules on the Schottky junction. At this point, compared to the tunneling current, which constitutes the majority of the channel current, the thermal emission current variation caused by the energy band changes induced by the charged NH_3 molecules in the channel region is minimal. Therefore, the carrier can still tunnel through the Schottky barrier, and there is essentially no change in the channel current.

In brief, the result indicates that Schottky barrier modulation by adsorbed NH_3 molecules at the metal/SiNW contact plays a dominant role in the Schottky-contacted SiNW FET ammonia sensor at room temperature. The dynamic alteration of the Schottky barrier thickness in response to the inflow or outflow of reductive NH_3 gas is a critical factor. It directly influences the probability of carrier tunneling across the barrier, thereby determining the observed change in the tunneling current. This sensing mechanistic insight highlights the response sensitivity of the sensor, which is crucial for its potential applications in gas sensing and biosensing.

Reversibility, Response Time, Stability, and Selectivity. Figure 5a illustrates the response characteristics of the SiNW FET sensor to 12.5 ppm of NH_3 during three cycles. It was evident that as the cycles of NH_3 gas inflow and outflow increased, the response and response speed of the sensor decreased. This could be attributed to the fact that residual NH_3 molecules that have not undergone electron transfer were not desorbed from the region of the metal/SiNW contact, thereby preventing the efficient absorption of subsequent NH_3 molecules. Additionally, a notable disadvantage of sensors dominated by the Schottky barrier is their typical lengthy recovery process at room temperature.[30] Compared with other the reported NH_3 gas sensors[25,32−3334,41−424344454647] (Figure 5b and Table S2), this SiNW FET ammonia sensor also exhibited rapid response, benefiting from ultrathin SiNWs with D_{NW} < 30 nm. The response time required for the response of the sensor to reach 5 and 50% was 7.9 and 85.8 s, respectively, at the first cycle (located in the red rectangle in Figure 5a). As shown in Figure 5c, the response of the sensor to 12.5 ppm of NH_3 remained at 67.8 and 60.3% (Figure S3), even after 1 month and 3 months, individually, demonstrating good stability with a low drift of −0.19% per day. To check the selectivity of the SiNW FET sensor for NH_3, responses of the sensor for common interfering VOC gases were also studied (Figure 5d). The results demonstrated that when the sensor was exposed to 25 ppm of NH_3, it exhibited a remarkable response of up to 91.4%. Furthermore, when the sensor encountered 25 ppm ethanol, isopropanol, and acetone, respectively, the current was observed to be slightly influenced by environmental noise, thereby highlighting excellent selectivity. This may be attributed to the fact that these VOC gases only display redox properties under specific conditions, not leading to electron transfer and thus not affecting the conductivity of the sensor at room temperature.

https://doi.org/10.1021/acssensors.4c02426
ACS Sens. 2024, 9, 6284−6291

CONCLUSIONS

In summary, we have fabricated high-performance SiNW FET ammonia sensors, based on precisely controlled high-density ultrathin SiNW channels grown on guiding terrace multisteps. A rather stable room-temperature NH_3 sensing has been accomplished with a response of 96.9% @ 25 ppm (or 38.6% at 2.5 ppm), a rapid response time of 7.9 s for 5% response (85.8 s for 50% response), and superior selectivity against common VOC gases. For the first time, the active field-effect sensing mechanism has been identified, that is, the field-effect modulation of metal/SiNW Schottky contact by the adsorbed NH_3 molecules, which plays a dominant role for this label-free SiNW FET ammonia sensor operating at room temperature. These results indicate that the ultrathin catalytic SiNWs are ideal and advantageous 1D channels for batch manufacturing and integrating high-performance and flexible gas sensors.

ASSOCIATED CONTENT

Supporting Information

The Supporting Information is available free of charge at https://pubs.acs.org/doi/10.1021/acssensors.4c02426.

Photo of gas sensing testing system, gas sensing properties of sensors under various bottom gate voltage and performance comparison tables (PDF)

AUTHOR INFORMATION

Corresponding Author

Linwei Yu − *School of Electronic Science and Engineering/National Laboratory of Solid-State Microstructures, Nanjing University, 210023 Nanjing, China;* orcid.org/0000-0002-0801-5210; Email: yulinwei@nju.edu.cn

Authors

Chunsheng Yang − *School of Electronic Science and Engineering/National Laboratory of Solid-State Microstructures, Nanjing University, 210023 Nanjing, China*

Wei Liao − *School of Electronic Science and Engineering/National Laboratory of Solid-State Microstructures, Nanjing University, 210023 Nanjing, China;* orcid.org/0009-0006-8804-9395

Junzhuan Wang − *School of Electronic Science and Engineering/National Laboratory of Solid-State Microstructures, Nanjing University, 210023 Nanjing, China*

Complete contact information is available at: https://pubs.acs.org/10.1021/acssensors.4c02426

Notes

The authors declare no competing financial interest.

ACKNOWLEDGMENTS

The authors acknowledge the financial support received from the National Key Research Program of China under granted No. 92164201, National Natural Science Foundation of China for Distinguished Young Scholars No. 62325403, and the Fundamental Research Funds for the Central Universities.

REFERENCES

(1) Kwak, D.; Lei, Y.; Maric, R. Ammonia Gas Sensors: A Comprehensive Review. *Talanta* **2019**, *204*, 713−730.

(2) Majhi, S.-M.; Mirzaei, A.; Kim, H.-W.; Kim, S. S.; Kim, T. W. Recent Advances in Energy-saving Chemiresistive Gas Sensors: A Review. *Nano Energy* **2021**, *79*, No. 105369.

(3) Šutka, A.; Gross, K. A. Spinel Ferrite Oxide Semiconductor Gas Sensors. *Sens. Actuators, B* **2016**, *222*, 95−105.

(4) Yao, M. S.; Li, W. H.; Xu, G. Metal−organic Frameworks and Their Derivatives for Electrically-transduced Gas Sensors. *Coord. Chem. Rev.* **2021**, *426*, No. 213479.

(5) Khan, M. A. H.; Rao, M. V.; Li, Q. Recent Advances in Electrochemical Sensors for Detecting Toxic Gases: NO_2, SO_2 and H_2S. *Sensors* **2019**, *19* (4), 905.

(6) Liao, Z.; Wang, Y.; Yuan, Z.; Gao, H.; Meng, F. Enhanced Optical Sensing of Butanone Gas Using CuOHF Nanosheet-Modified Fiber Optic Evanescent-Wave Absorption Sensor. *IEEE Trans. Instrum. Meas.* **2024**, *73*, 1−12.

(7) Wang, Y.; Yan, C.; Liang, C.; Liu, Y.; Li, H.; Zhang, C.; Duan, X.; Pan, Y. Sensitive Materials Used in Surface Acoustic Wave Gas Sensors for Detecting Sulfur-Containing Compounds. *Polymers* **2024**, *16* (4), 457.

(8) Demami, F.; Ni, L.; Rogel, R.; Salaun, A. C.; Pichon, L. Silicon Nanowires Based Resistors as Gas Sensors. *Sens. Actuators, B* **2012**, *170*, 158−162.

(9) Zhu, L. S.; Zhang, J.; Xu, X. W.; Yu, Y. Z.; Wu, X.; Yang, T.; Wang, X. H. Room Temperature H_2 Detection Based on Pd/SiNWs/p-Si Schottky Diode Structure. *Sens. Actuators, B* **2016**, *227*, 515−523.

(10) Jung, G.; Hong, S.; Shin, W.; Jeong, Y.; Park, J.; Kim, D.; Lee, J.-H. Design Optimization of FET-type Gas Sensor Considering Device Characteristics, Sensitivity, Power, Noise, and SNR. *Sens. Actuators, B* **2022**, *369*, No. 132257.

(11) Mao, S.; Chang, J.; Pu, H.; Lu, G.; He, Q.; Zhang, H.; Chen, J. Two-dimensional Nanomaterial-based Field-effect Transistors for Chemical and Biological Sensing. *Chem. Soc. Rev.* **2017**, *46* (22), 6872−6904.

(12) Wang, B.; Cancilla, J. C.; Torrecilla, J. S.; Haick, H. Artificial Sensing Intelligence with Silicon Nanowires for Ultraselective Detection in the Gas Phase. *Nano Lett.* **2014**, *14* (2), 933−938.

(13) Liu, C.; Hu, J.; Wu, G.; Cao, J.; Zhang, Z.; Zhang, Y. Carbon Nanotube-Based Field-Effect Transistor-Type Sensor with a Sensing Gate for ppb-Level Formaldehyde Detection. *ACS Appl. Mater. Interfaces* **2021**, *13* (47), 56309−56319.

(14) Sharma, B.; Sharma, A.; Kim, J.-S. Recent Advances on H_2 Sensor Technologies Based on MOX and FET Devices: A review. *Sens. Actuators, B* **2018**, *262*, 758−770.

(15) Sharma, B.; Kim, J.-S. MEMS Based Highly Sensitive Dual FET Gas Sensor Using Graphene Decorated Pd-Ag Alloy Nanoparticles for H_2 Detection. *Sci. Rep.* **2018**, *8* (1), No. 5902.

(16) Wang, B.; Li, H.; Tan, H.; Gu, Y.; Chen, L.; Ji, L.; Sun, Z.; Sun, Q.; Ding, S.; Zhang, D. W.; Zhu, H. Gate-Modulated High-Response Field-Effect Transistor-Type Gas Sensor Based on the MoS2/Metal−Organic Framework Heterostructure. *ACS Appl. Mater. Interfaces* **2022**, *14* (37), 42356−42364.

(17) Raman, S.; A, R. S.; M, S. Advances in Silicon Nanowire Applications in Energy Generation, Storage, Sensing, and Electronics: A Review. *Nanotechnology* **2023**, *34* (18), No. 182001.

(18) Akbari-Saatlu, M.; Procek, M.; Mattsson, C.; Thungström, G.; Nilsson, H.-E.; Xiong, W.; Xu, B.; Li, Y.; Radamson, H. H. Silicon Nanowires for Gas Sensing: A Review. *Nanomaterials* **2020**, *10* (11), 2215.

(19) Choi, B.; Ahn, J.-H.; Lee, J.; Yoon, J.; Lee, J.; Jeon, M.; Kim, D. M.; Kim, D. H.; Park, I.; Choi, S.-J. A Bottom-gate Silicon Nanowire Field-effect Transistor with Functionalized Palladium Nanoparticles for Hydrogen Gas Sensors. *Solid-State Electron.* **2015**, *114*, 76−79.

(20) Zhiyong, F.; Lu, J. G. Chemical Sensing with ZnO Nanowire Field-effect Transistor. *IEEE Trans. Nanotechnol.* **2006**, *5* (4), 393−396.

(21) Zhang, H.; Kikuchi, N.; Ohshima, N.; Kajisa, T.; Sakata, T.; Izumi, T.; Sone, H. Design and Fabrication of Silicon Nanowire-Based Biosensors with Integration of Critical Factors: Toward Ultrasensitive Specific Detection of Biomolecules. *ACS Appl. Mater. Interfaces* **2020**, *12* (46), 51808−51819.

(22) Yu, L.; Alet, P.-J.; Picardi, G.; Roca i Cabarrocas, P. An In-Plane Solid-Liquid-Solid Growth Mode for Self-Avoiding Lateral Silicon Nanowires. *Phys. Rev. Lett.* **2009**, *102* (12), No. 125501.
(23) Xue, Z.; Xu, M.; Zhao, Y.; Wang, J.; Jiang, X.; Yu, L.; Wang, J.; Xu, J.; Shi, Y.; Chen, K.; Roca i Cabarrocas, P. Engineering Island-chain Silicon Nanowires via a Droplet Mediated Plateau-Rayleigh Transformation. *Nat. Commun.* **2016**, *7* (1), No. 12836.
(24) Sun, Y.; Dong, T.; Yu, L.; Xu, J.; Chen, K. Planar Growth, Integration, and Applications of Semiconducting Nanowires. *Adv. Mater.* **2019**, *32* (27), No. 1903945.
(25) Song, X.; Hu, R.; Xu, S.; Liu, Z.; Wang, J.; Shi, Y.; Xu, J.; Chen, K.; Yu, L. Highly Sensitive Ammonia Gas Detection at Room Temperature by Integratable Silicon Nanowire Field-Effect Sensors. *ACS Appl. Mater. Interfaces* **2021**, *13* (12), 14377−14384.
(26) Kim, D.; Park, C.; Choi, W.; Shin, S.-H.; Jin, B.; Baek, R.-H.; Lee, J.-S. Improved Long-Term Responses of Au-Decorated Si Nanowire FET Sensor for NH_3 Detection. *IEEE Sens. J.* **2020**, *20* (5), 2270−2277.
(27) Xu, S.; Hu, R.; Wang, J.; Li, Z.; Xu, J.; Chen, K.; Yu, L. Terrace-confined Guided Growth of High-density Ultrathin Silicon Nanowire Array for Large Area Electronics. *Nanotechnology* **2021**, *32* (26), No. 265602.
(28) Hu, R.; Xu, S.; Wang, J.; Shi, Y.; Xu, J.; Chen, K.; Yu, L. Unprecedented Uniform 3D Growth Integration of 10-Layer Stacked Si Nanowires on Tightly Confined Sidewall Grooves. *Nano Lett.* **2020**, *20* (10), 7489−7497.
(29) Hu, R.; Liang, Y.; Qian, W.; Gan, X.; Liang, L.; Wang, J.; Liu, Z.; Shi, Y.; Xu, J.; Chen, K.; Yu, L. Ultra-Confined Catalytic Growth Integration of Sub-10 nm 3D Stacked Silicon Nanowires Via a Self-Delimited Droplet Formation Strategy. *Small* **2022**, *18* (42), No. 2204390.
(30) Peng, N.; Zhang, Q.; Chow, C. L.; Tan, O. K.; Marzari, N. Sensing Mechanisms for Carbon Nanotube Based NH_3 Gas Detection. *Nano Lett.* **2009**, *9* (4), 1626−1630.
(31) Wang, J. X.; Sun, X. W.; Yang, Y.; Huang, H.; Lee, Y. C.; Tan, O. K.; Vayssieres, L. Hydrothermally Grown Oriented ZnO Nanorod Arrays for Gas Sensing Applications. *Nanotechnology* **2006**, *17* (19), 4995−4998.
(32) Le, Q. T.; Shikoh, A. S.; Kang, K.; Lee, J.; Kim, J. Room-Temperature Sub-ppm Detection and Machine Learning-Based High-Accuracy Selective Analysis of Ammonia Gas Using Silicon Vertical Microwire Arrays. *ACS Appl. Electron. Mater.* **2023**, *5* (1), 357−366.
(33) Nath, P.; Sarkar, D. Ammonia Sensing by Silicon Nanowires (SINWs) Obtained Through Metal Assisted Electrochemical Etching. *Mater. Today: Proc.* **2022**, *57*, 224−227.
(34) Wan, J.; Deng, S.-R.; Yang, R.; Shu, Z.; Lu, B.-R.; Xie, S.-Q.; Chen, Y.; Huq, E.; Liu, R.; Qu, X.-P. Silicon Nanowire Sensor for Gas Detection Fabricated by Nanoimprint on $SU8/SiO_2$/PMMA Trilayer. *Microelectron. Eng.* **2009**, *86* (4−6), 1238−1242.
(35) Yeh, Y.-M.; Chang, S.-J.; Wang, P. H.; Hsueh, T.-J. A Room-Temperature TiO_2-based Ammonia Gas Sensor with Three-Dimensional Through-Silicon-Via Structure. *ECS J. Solid State Sci. Technol.* **2022**, *11* (6), No. 067002.
(36) Jaiswal, M.; Kumar, R.; Mittal, J.; Jha, P. Synthesis of CrO_3 Intercalated Multilayer Graphene for Rapid and Reversible NH_3 Gas Sensing. *Sens. Actuators, B* **2020**, *310*, No. 127826.
(37) Gai, S.; Wang, B.; Wang, X.; Zhang, R.; Miao, S.; Wu, Y. Ultrafast NH_3 Gas Sensor Based on Phthalocyanine-optimized Non-covalent Hybrid of Carbon Nanotubes with Pyrrole. *Sens. Actuators, B* **2022**, *357*, No. 131352.
(38) Falak, A.; Tian, Y.; Yan, L.; Xu, L.; Song, Z.; Hu, H.; Dong, F.; Adamu, B. I.; Zhao, M.; Chen, P.; Wang, H.; Chu, W. Ultrathin MoO_x/Graphene Hybrid Field Effect Transistor Sensors Prepared Simply by a Shadow Mask Approach for Selective ppb-Level NH3 Sensing with Simultaneous Superior Response and Fast Recovery. *ACS Appl. Mater. Interfaces* **2020**, *7* (10), No. 1902002.
(39) Verma, A.; Sahu, P. K.; Chaudhary, V.; Singh, A. K.; Mishra, V. N.; Prakash, R. Fabrication and Characterization of P3HT/MoS_2 Thin-Film Based Ammonia Sensor Operated at Room Temperature. *IEEE Sens. J.* **2022**, *22* (11), 10361−10369.
(40) Gautam, S. K.; Panda, S. Field Effect Characteristics and Gas Sensing Properties of Vertically Grown PANI Nanofibers. *Org. Electron.* **2023**, *123*, No. 106938.
(41) Barandun, G.; Soprani, M.; Naficy, S.; Grell, M.; Kasimatis, M.; Chiu, K. L.; Ponzoni, A.; Güder, F. Cellulose Fibers Enable Near-Zero-Cost Electrical Sensing of Water-Soluble Gases. *ACS Sens.* **2019**, *4* (6), 1662−1669.
(42) Kumar, R.; Kumar, A.; Singh, R.; Kashyap, R.; Kumar, R.; Kumar, D.; Sharma, S. K.; Kumar, M. Room Temperature Ammonia Gas Sensor Using Meta Toluic Acid Functionalized Graphene Oxide. *Mater. Chem. Phys.* **2020**, *240*, No. 121922.
(43) Ansari, N.; Lone, M. Y.; Ali, J.; Husain, M.; Husain, S. Enhancement of Gas Sensor Response Characteristics of Functionalized SWCNTs. In *Proceedings of International Conference on Recent Trends in Mechanical and Materials Engineering: ICRTMME 2019*, 2020.
(44) Kumar, R.; Singh, R.; Kumar, A.; Kashyap, R.; Kumar, D.; Kumar, M. Chemically Functionalized Graphene Oxide Thin Films for Selective Ammonia Gas Sensing. *Mater. Res. Express* **2020**, *7* (1), No. 015612.
(45) Lee, B. H.; Kim, S.; Lee, S. Y. Ammonia Gas Sensing Properties of 6,13-Bis(tri-isopropylsilyethynyl) Pentacene Based Field-Effect Transistor. *Trans. Electr. Electron. Mater.* **2022**, *23* (2), 182−186.
(46) Tohidi, S.; Parhizkar, M.; Bidadi, H.; Mohamad-Rezaei, R. High-performance Chemiresistor-type NH_3 Gas Sensor Based on Three-dimensional Reduced Graphene Oxide/Polyaniline Hybrid. *Nanotechnology* **2020**, *31* (41), No. 415501.
(47) Zhao, M.; Tian, Y.; Yan, L.; Liu, R.; Chen, P.; Wang, H.; Chu, W. Unique Modulation Effects on the Performance of Graphene-based Ammonia Sensors via Ultrathin Bimetallic Au/Pt Layers and gate Voltages. *Phys. Chem. Chem. Phys.* **2023**, *25* (29), 19764−19772.

https://doi.org/10.1021/acssensors.4c02426
ACS Sens. 2024, 9, 6284−6291